ACS APPLIED MATERIALS & INTERFACES

Research Article

www.acsami.org

Insights into Size-Dominant Magnetic Microwave Absorption Properties of CoNi Microflowers via Off-Axis Electron Holography

Qinghe Liu,[†,§] Qi Cao,[†,§] Xuebing Zhao,[†] Han Bi,[†] Chao Wang,[†] David Sichen Wu,[‡] and Renchao Che*[,†]

[†]Laboratory of Advanced Materials, Department of Materials Science, Collaborative Innovation Center of Chemistry for Energy Materials, Fudan University, Shanghai 200438, People's Republic of China

[‡]Georgia Institute of Technology, Atlanta, Georgia 30332-0245, United States

Supporting Information

ABSTRACT: In this study, CoNi flower-like hierarchical microstructures with different sizes were obtained via a one-step solvothermal method by simply adjusting the concentration of precursors and surfactant. The obtained CoNi microflowers possess uniform and tunable size, good monodispersity, and remarkable magnetic microwave absorption properties as well as electron holography phase images. Characterization results have demonstrated the dependency of properties of CoNi microflowers on their morphologies and sizes. The microflowers exhibit different stray magnetic fields that might be determined by whether the pristine nanoflakes on the flowers' surface was parallel or perpendicular to grid plane. And as the size of microflowers increased, the coercive force (Hc) value decreased while saturation magnetization (Ms) value gradually increased, and it can be also observed that the values of Ms and Hc at 5 K are higher than those at 300 K. In addition, the blocking temperature decreased when size increased. Typically, the 2.5 μm CoNi microflowers achieve the maximum reflection loss (RL) value of −28.5 dB at 6.8 GHz with a thickness of 2 mm, while on the other hand, the 0.6 μm flowers achieved a broader absorption bandwidth below −10 dB of 6.5 GHz. Therefore, it is believable that the CoNi flowers with different sizes and hierarchical structures in this work have great potential for high performance magnetic microwave absorption applications.

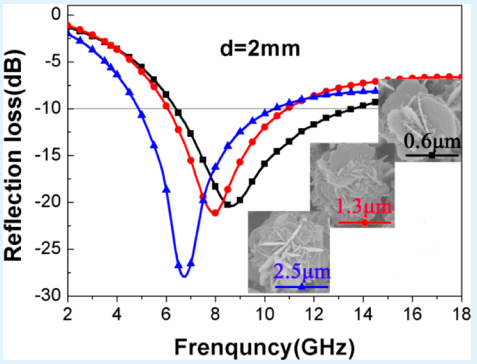

KEYWORDS: *CoNi microflowers, particle size, microwave absorption, magnetism, electron holography*

1. INTRODUCTION

Recently, electromagnetic (EM) interference shielding has become an important topic for researchers due to the rapid increase of telecommunications equipment and the demand for anticontamination devices for EM signals. Magnetic composites can be utilized as efficient EM wave absorption materials owning to their dissipation effects for electrons and phonons via periodical boundary conditions within nanostructures.[1−5]

Transition metals cobalt (Co) and nickel (Ni) and their bimetallic alloy nanostructures have attracted a considerable attention attributed to their potentiality for applications in many fields like microwave absorption,[6,7] catalysis,[8−10] biomedical devices[11] and also magnetic resonance imaging contrast agents.[12] Particle size and composition, as well as surface structures, are all crucial factors for physical and chemical properties of CoNi alloys. To achieve highly tunable chemical structures and composition, it is a prerequisite to understand their structures at molecular level . Until now, great efforts have been focused on controlling the morphologies and size of composite materials to obtain demanded surface properties.[13−16] Our group has previously studied the facile adjustment of microwave absorption properties of CoNi alloys by controlling their surface morphologies and discovered that the hierarchical flower-like CoNi particles demonstrated the most favorable capability to enhance surface scattering microwave absorption.[17] Nevertheless, the efficient size-controllable synthesis, as well as tuning the dependence of microwave absorption properties of CoNi alloy microflowers of different size toward EM shielding applications, is still rather limited.

In the paper, we report the synthesis of CoNi microflowers with different sizes of 0.6, 1.3, and 2.5 μm in sodium hydroxide and ethylene glycol solution, and it seems that the morphologies and size of CoNi microflowers depended strongly on concentration of precursor solutions and surfactant. Here in particular, we focused on the surface nanoflakes of CoNi flowers, whose shapes and size changed obviously along with the concentration of Co(II) and Ni(II) precursors in solution. In addition, the microwave absorption capacity also depended on the size of CoNi microflowers, which might be attributed to the strength of different stray magnetic fields demonstrated by off-axis electron holography. In this regard, the different sizes of obtained CoNi microflowers have been analyzed and consequently associated with the hysteresis loops as well as field cooling and zero-field cooling (FC/ZFC) curves systematically. Thus, eventually, the relationship between

Received: December 3, 2014
Accepted: February 2, 2015
Published: February 2, 2015

DOI: 10.1021/am508527s
ACS Appl. Mater. Interfaces 2015, 7, 4233−4240

particle size, magnetic properties, and microwave absorption abilities of as-obtained CoNi microflowers was revealed by electron holography and discussed in detail in this article.

2. EXPERIMENTAL SECTION

2.1. Materials. All chemicals including Nickel(II) acetate tetrahydrate (≥98.0%), cobalt(II) acetate tetrahydrate (≥99.5%), ethylene glycol (EG, ≥99%), sodium hydroxide (NaOH, ≥96%), absolute ethanol (≥99.7), and hexadecyl trimethylammonium bromide (CTAB, AR) were purchased from Sinopharm Chemical Reagent Co., Ltd. and used as received without further purification. In all experiments, deionized water obtained from Milli-Q system (Millipore, Bedford, MA) was used.

2.2. Synthetic Procedures. The CoNi microflowers were prepared in a solvothermal system as follows. Cobalt(II) and nickel(II) acetate hydrate were utilized as precursors and dissolved at first in a EG solution where the concentration of NaOH and surfactant CTAB were varied in the range of 0−3 M, while the concentration of precursors was in the range of 0−0.25 M with a Co/Ni molar ratio of 1/4. The mixture was stirred and dissolved at room temperature, and then transferred into a Teflon-lined stainless-steel autoclave (50 mL capacity). Afterward, the autoclave was sealed and maintained at 200 °C for several hours. And when the autoclave naturally cooled down to room temperature at last, the products as black-gray powders were collected and washed with either distilled water or absolute ethanol, and dried at 60 °C in a vacuum oven for further characterization.

2.3. Characterization. The morphologies and sizes of the CoNi alloy particles were characterized using a field-emission scanning electron microscope (FE-SEM, Hitachi S-4800, Japan). The powder X-ray diffraction (XRD) patterns were recorded on a X-ray diffractometer (Bruker D8, Germany) with Ni-filtered Cu Kα radiation working at 40 kV and 40 mA. Magnetic properties were determined with a superconducting quantum interference device (SQUID, Quantum Design MPMS, USA). Typically, 5−10 mg of our powder samples was capsuled in plastic encapsulant for the magnetization hysteresis loops measurements. The microstructural information, as well as electron holographic observation of as-prepared products, was achieved using a field-emission transmission electron microscope (FE-TEM, JEOL JEM-2100F, Japan) equipped with a postcolumn Gatan imaging filter (GIF, Tridium 863) system working at 200 kV.

2.4. Measurements of EM Parameters. Microwave absorption properties were studied by dispersing the samples into epoxy resin (EP) with a weight ratio of 1:5. A portion of the composite was coated on an aluminum substrate (180 mm × 180 mm) with a thickness of 2 mm to measure the reflection loss of the samples. The remaining sample was molded into the hollow pipe of a rectangular waveguide cavity with dimensions of 10.2 mm × 2.9 mm × 1.2 mm for complex permittivity and permeability measurements. In all experiments, the complex relative permittivity, permeability and reflection loss values were obtained with a HP8510C vector network analyzer in 2−18 GHz frequency range.

2.5. Electron Holography Analysis. Electron holography observation was carried out with a JEM 2100F TEM. A electrostatic biprism (a thin conducting wire) system was installed into the microscope column perpendicular to the electron beam to minimize the image disturbances from Fresnel diffraction fringes by independently controlling the fringe spaces and the width of the interference region. The application of a voltage to the biprism results in overlap of the electron wave to create an interference fringe pattern. The conditions of the lens system were adjusted to obtain appropriate magnifications for the sample and electron holograms. The residual magnetic field at the sample position was estimated to be $<1 \times 10^{-5}$ T using the electron microscope lens design codes based on the finite-element method, with shapes and properties of lens materials as input parameters. The vacuum reference holograms was obtained from the vacuum alone by removing the specimen from the field of view without changing the electron-optical parameters of the microscope.

3. RESULTS AND DISCUSSION

The compositions of as-synthesized samples were identified by XRD characterization. Figure 1 shows the XRD pattern of as-obtained CoNi microflower sample. The sharp diffraction peaks at 44.5°, 51.8°, 76.7°, and 92.7° can be indexed to (111), (200), (220), and (311) crystal planes, respectively, which might be planes of either Ni or Co with a face-center cubic (fcc) structure (PDF#O4-0850 and PDF#15-0806). There are no characteristic peaks of nickel/cobalt oxides and hydroxides can be observed, which demonstrates the phase purity of as-synthesized microflowers. In addition, it could also be observed from the magnified XRD patterns of the (111) and (200) crystal planes (Figure S1 of the Supporting Information) that the peak positions of the obtained CoNi microflowers typically lie between the positions of pure Ni and pure Co phase, further revealing that Co atoms and Ni atoms have entered into each other's crystal lattices and finally formed alloyed phase.

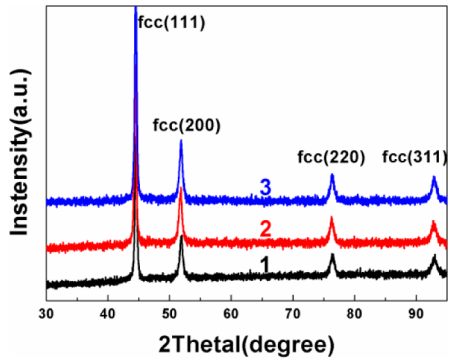

Figure 1. XRD patterns of CoNi microflowers of different sizes (1:0.6, 2:1.3, and 3:2.5 μm).

Typically, CoNi alloy microflowers of three different sizes (i.e., 0.6, 1.3, and 2.5 μm) were achieved and investigated in this work. Figure 2 shows the energy dispersive X-ray spectroscopy (EDS) characterization results of CoNi microflowers of 1.3 μm. Figure 2d reveals that the atomic percentage (atom %) of Co and Ni is about 17.10% and 82.90%, respectively, which is quite approximate to the added amount of cobalt and nickel precursors (1:4). Also, the SEM/EDS and STEM elemental mapping images in Figure 2a−c and Figure S2 of the Supporting Information display the distribution of each element on the surface and in the interior within a single particle, suggesting that both cobalt and nickel possess rather

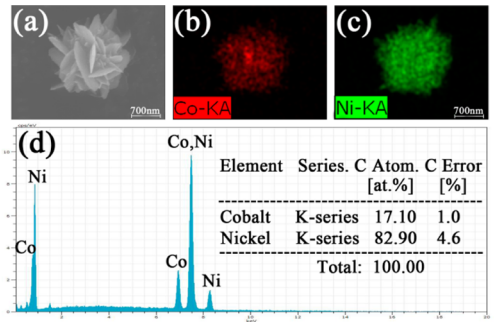

Figure 2. (a−c) SEM/EDS elemental mapping profiles of Co (b) and Ni (c) of a single particle (a). (d) EDS spectrum of the 1.3 μm CoNi microflowers.

DOI: 10.1021/am508527s
ACS Appl. Mater. Interfaces 2015, 7, 4233−4240

homogeneous spacial distributions despite the fact that a relatively low concentration of cobalt can be observed at the outer part of the particle, and this variation in composition might be ascribed to the small content of cobalt precursors (i.e., only a quarter of nickel). Besides, nearly the same results can be obtained as well from CoNi microflowers of other different sizes, as displayed in Figure S3 of the Supporting Information.

The representative selected area electron diffraction (SAED) pattern taken from an area containing a large amount of CoNi microflowers is shown in Figure 3a. It can be well indexed to be

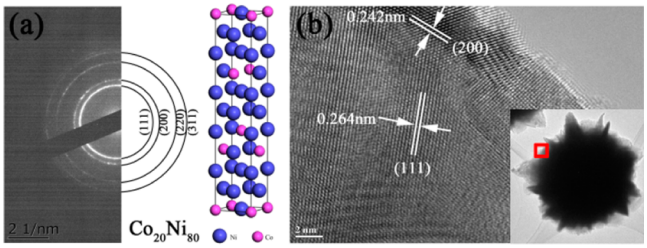

Figure 3. (a) SAED pattern of the CoNi microflowers. (b) HRTEM image of CoNi microflowers. Inset indicates the place where HRTEM image was taken from.

a typical fcc crystalline phase, with distinct inner diffraction rings corresponding to (111), (200), (220), and (311) crystalline planes. Moreover, Figure 3b displays the high-resolution TEM (HRTEM) image of the marginal area of a single CoNi microflower, in which the lattice fringes correspond to 0.26 nm of (111) plane and 0.242 nm of (200) plane of CoNi alloy flowers definitely.

On the basis of the combinatorial SEM and TEM analysis of Figure 4, it is confirmed that a series of CoNi microflowers with different sizes have been successfully achieved. The size of flowers can be controlled accurately by changing the concentration of the precursors and surfactant. Typically, when the concentration of precursors increased, the size became larger. However, the precursor concentration had little influence on the surface morphologies of obtained CoNi microflowers. Figure 4 shows the SEM images of the products synthesized with 0.01, 0.05, and 0.15 M of precursors addition, respectively. It can be seen that, although similar uniformity and monodispersity have been achieved (also shown in Figure S4 of Supporting Information), the pristine nanoflakes on surface turn smaller and denser, and the particle size can generally grow to as large as 3 μm as the concentration of precursors were increased. And when the concentration of precursors finally increased to 0.25 M, no evident shape and size changes could be observed any more. It is also of note that since the synthesis yield remained quite high (up to 95%), product amount at ultralarge scale can be achieved for practical applications.

On the other hand, the amount of CTAB as the surfactant is also crucial for obtaining CoNi microflowers of different sizes. As the concentration of CTAB increased, the size became smaller as well and the surface nanoflakes became larger but sparser, and sometimes there were only a few nanoflakes on surface, as shown in Figure S4a of Supporting Information. A probable formation mechanism of different morphologies of CoNi microflowers is proposed in Figure 5. Typically, the Co^{2+}

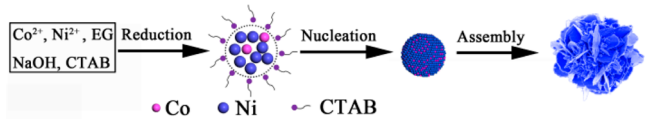

Figure 5. Schematic diagram of the reaction process.

and Ni^{2+} ions were reduced by EG to form Co and Ni atoms at first. Then, the primary nuclei of Co and Ni atoms diffused and aggregated, thus generating small CoNi nanoparticles. Afterward, CTAB molecules served as the soft templates so that CoNi nanoparticles with a broad size distribution agglomerated to micrometer-scale particles and were further shaped into hierarchical flower-like structures due to the wrap effects of a large quantity of adsorbed CTAB molecule chains. There was also a thermodynamic driving force for the nanoparticle

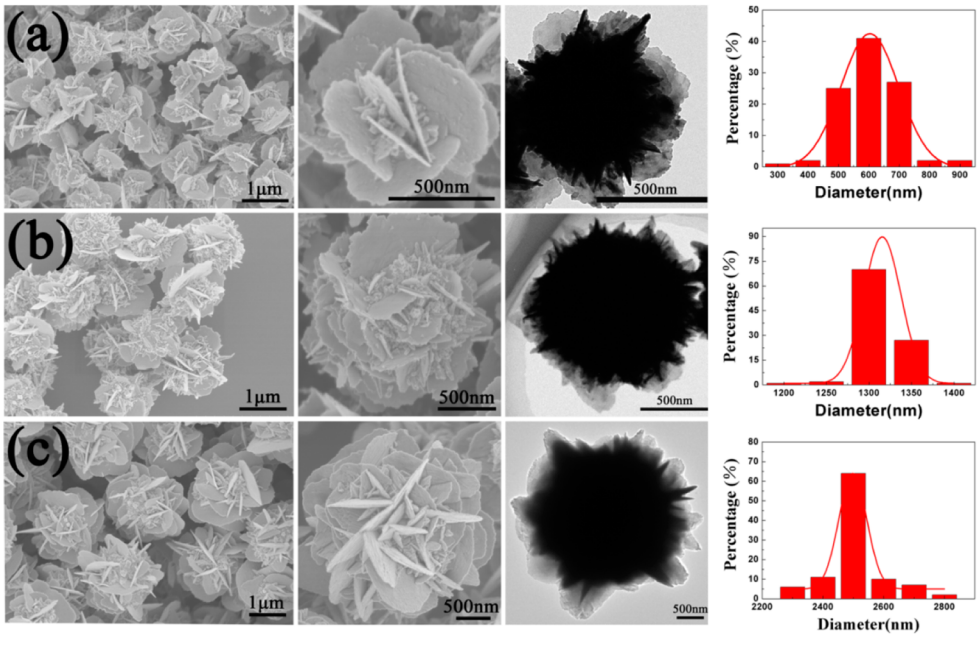

Figure 4. SEM, TEM, and size distribution histogram images of CoNi microflowers of different sizes: (a) 0.6 μm, (b) 1.3 μm, and (c) 2.5 μm.

DOI: 10.1021/am508527s
ACS Appl. Mater. Interfaces 2015, 7, 4233−4240

agglomeration since the surface energy could be reduced substantially when surface area was enlarged. Hence in this way, the small CoNi nanoparticles finally grew into large microflowers with the help of surfactant molecules. Furthermore, our results suggest that CTAB also had a special assembly effect on the size of the CoNi flowers as well.

Figure 6a shows the hysteresis loops of samples of different sizes measured at 300 K, indicating the ferromagnetic behavior

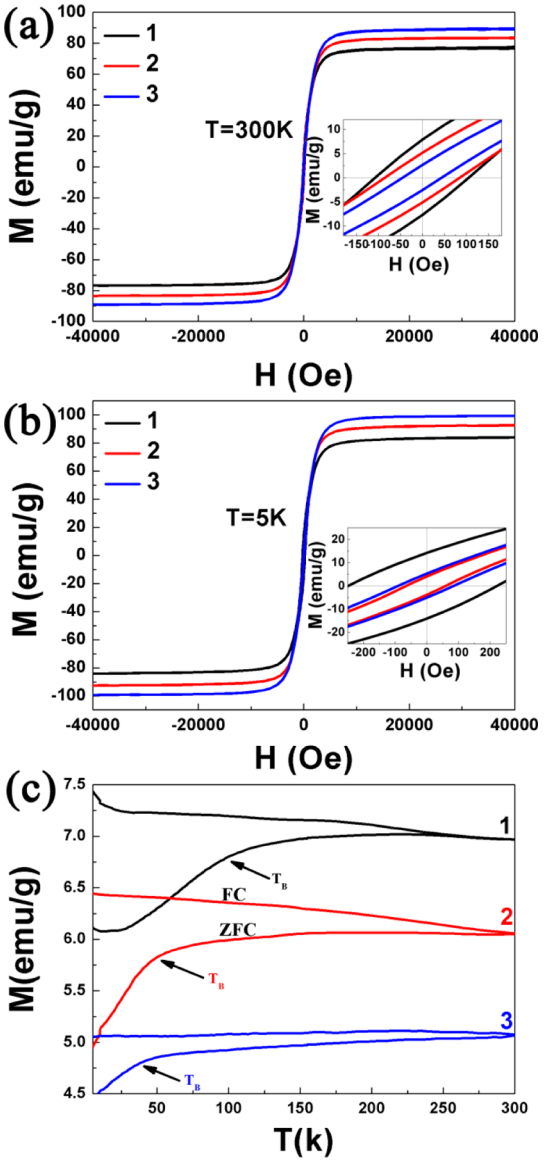

Figure 6. Hysteresis loops of CoNi microflowers measured at (a) 300 K and (b) 5 K. The insets give enlarged views of the hysteresis loops. (c) Field-cooled (FC) and zero-field-cooled (ZFC) curves for CoNi microflower of different sizes at 100 Oe. (1:0.6, 2:1.3, and 3:2.5 μm).

at room temperature of the CoNi microflowers. The hysteresis loops also reveal that the Ms values are 77.65, 83.60, and 89.45 emu/g and corresponding Hc values are 108.93, 85.72, and 46.72 Oe for 0.6, 1.3, and 2.5 μm flowers, respectively (Figure 8b). It can be deduced that as the size of CoNi microflowers increased, Hc values dropped off while Ms accelerated, which is consistent with the literature report.[18] Both the enlarged size and surface areas of larger CoNi flowers might have contributed to the increase of Ms value. And on the other hand, smaller CoNi microflowers exhibited significantly enhanced Hc values compared with larger ones, which may be probably due to stronger shape anisotropy originated from larger nanoflakes stacked on surface.

The low temperature hysteresis loops of CoNi microflowers are shown in Figure 6b. It is clear that typical ferromagnetic behavior was demonstrated at the temperature of 5 K as well. Besides, the Ms and Hc values are 83.99, 92.73, and 99.26 emu/g as well as 221.95, 86.08, and 60.49 Oe, respectively. It is evident that both Ms and Hc values at 5 K are higher than those at 300 K, which could be ascribed to thermal activation effect as the temperature increased according to the literature report.[19]

It is known to all that magnetic properties are sensitive to temperature. The blocking temperature (T_B) represents the temperature required for matters to overcome energy barrier via thermal activation. To study the magnetism of the samples further, the field cooling (FC)/zero-field cooling (ZFC) magnetization curves were recorded to illustrate the magnetism of CoNi microflowers within the field of 100 Oe (Figure 6c). As can be observed, when measuring temperature decreased from 300 to 5 K, the ZFC curves began to drop at a certain broad cusp temperature (i.e., T_B) and deviated from the FC magnetization curves finally. The broad cusps of 85−95, 60−70, and 40−50 K are observed for 0.6, 1.3, and 2.5 μm CoNi microflowers, respectively, suggesting a large magnetic anisotropy energy barrier distribution existed in the CoNi alloys. In addition, T_B decreased as the size increased, indicating that larger CoNi microflowers need less thermal energy to overcome energy barrier, which could be attributed to the larger size distribution and dipolar interactions among pristine surface nanoflakes.[2,20]

Figure 7 shows the phase images reconstructed from the electron holograms with the amplification factor of 4. The spacing between adjacent equiphase lines reveals a phase shift value of $\pi/2$. Overall, the CoNi microflower exhibit relatively complex surface magnetic configurations. For one thing, it possesses strong stray magnetic lines whose flow direction

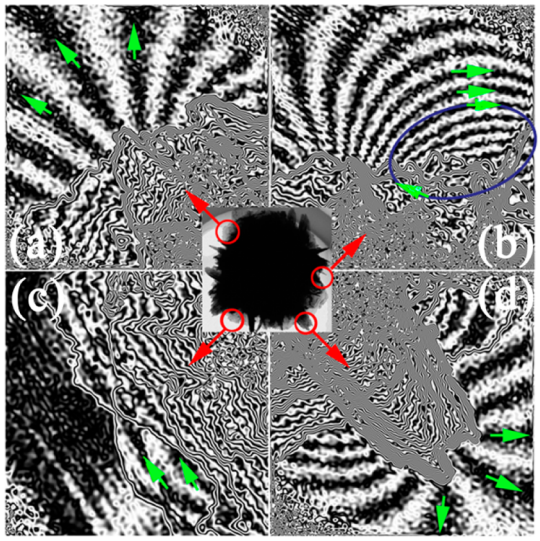

Figure 7. (a) Strong stray magnetic lines and (b) closed magnetic flux lines of CoNi microflowers. (c) The magnetic field of pristine nanoflakes which are parallel to the plane and (d) the stray magnetic flux lines of the nanoflakes which are perpendicular to the plane.

DOI: 10.1021/am508527s
ACS Appl. Mater. Interfaces 2015, 7, 4233−4240

contours extend to the infinity (Figure 7a). For another, it also has closed magnetic flux lines derived from the dipolar fields, which return back to the sample itself (Figure 7b). The closed magnetic flux lines have made an intense magnetic interaction between every two neighboring nanoflakes. Further, to illustrate the magnetic coupling characters within areas of several dozens of nanometers, the pristine nanoflakes embedding on the surface of CoNi microflowers are examined in particular. Figure 7c displays the magnetic field of nanoflakes which are relatively parallel to the plane of TEM grid. It can be observed that there is no stray magnetic flux lines, but only the flux lines resulted from the interior of the nanoflakes existing, owing to the very small thickness of about 20 nm of the nanoflakes. The magnetic flux lines will become stronger and more obvious with an amplification factor of 10, as shown in Figure S5 of Supporting Information. Finally, Figure 7d displays the case of nanoflakes which are nearly perpendicular to the plane, and there are quite strong stray magnetic flux lines can be seen clearly here.

The stray fields are essentially dependent on the dipole arrangement on the materials' surface structures, which in turn is affected by local geometries of materials. The strong stray magnetic fields of CoNi microflowers could be attributed to their pristine surface nanoflakes. Due to the large aspect ratio of the nanoflakes, the magnetic field intensity at the margins of the nanoflakes is distinctly concentrated under irradiation of EM wave along the alternated polarization vector direction. Thus, it is reasonable that these concentrated margins will act as the multipoles coupled with the incident magnetic field according to EM resonance effect, and bring about the strong stray magnetic fields and microwave absorption ability as a result. And in this regard, our electron holography analysis has provided novel insights for understanding magnetic and microwave absorption properties of the CoNi hierarchical microflowers.

The microwave reflection loss (RL) values were calculated using the relative complex permittivity and permeability at a given frequency and layer thickness according to the transmit line theory.[21] Figure 8 presents the calculated results of the curves for frequency dependence of RL of the samples of different size. It can be found that the 2.5 μm microflowers exhibit the strongest microwave absorption intensity compared with the others at all thicknesses of 2, 3, 4, and 5 mm. The maximum RL value (RL_{max}) of 2.5 μm CoNi microflower sample is −28.5 dB at 6.8 GHz with a thickness of 2 mm, while the maximum absorption bandwidths of about 6.5 dB is achieved by 0.6 μm microflowers at the thickness of 2 mm (Figure 8a). The peak values of RL_{max} get enhanced and the corresponding frequency band shift to lower frequency region as the size of CoNi microflowers increased. In addition, the absorption band shifts as well to lower frequency range if the absorber thickness increased when measuring. Hence, it is supposed that increased size of CoNi microflowers and absorber thickness are in favor of lower frequency absorbers, while on the contrary, small particle size and thin thickness will do well for higher frequency absorbers. Besides, since different sizes lead to different frequency absorption bands, it is possible for us to construct a full absorption system by making them composites of CoNi flowers of different sizes.

It is supposed that the strong absorption ability of the CoNi microflowers results from their hierarchical structures of surface nanoflakes. First, their large exposed surfaces have led to strong interfacial magnetic dipole interaction, as reflected by the stray fields of the electron hologram, and brought about an excellent microwave absorption capability subsequently. Second, for each CoNi single microflower, there is an assembly tendency of surface nanoflakes with different density distributions to scatter or absorb the propagated microwave, resulting in repeated absorption and exhaustion. Besides, the propagated microwave might be multiply scattered in the space woven by nanoflakes as well, and hence, energy attenuation via the network of numerous overlapping nanoflakes gets enhanced, which has further resulted in larger microwave absorption intensities. Moreover, owing to the fact that the size of CoNi microflowers can be accurately controlled by polyol process, it seems convenient for us to obtain granular materials of the CoNi

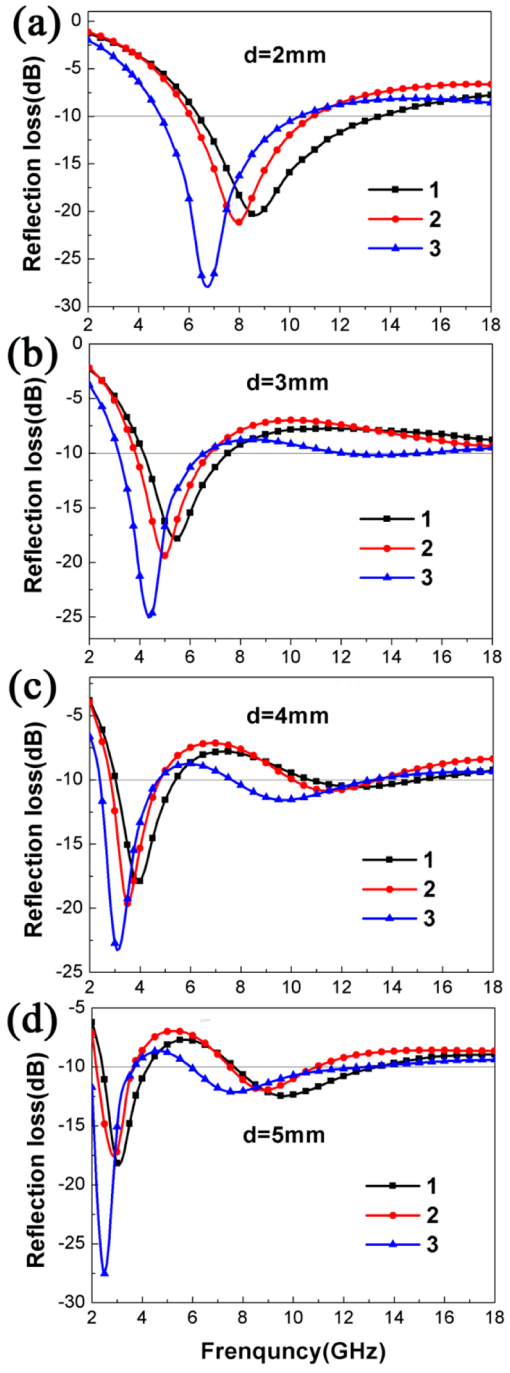

Figure 8. Microwave RL curves of CoNi flowers (1:0.6, 2:1.3, and 3:2.5 μm) at different thicknesses: (a) d = 2 mm, (b) d = 3 mm, (c) d = 4 mm, and (d) d = 5 mm.

DOI: 10.1021/am508527s
ACS Appl. Mater. Interfaces 2015, 7, 4233−4240

microflowers with optimized absorption characteristics in demanded microwave frequency regions by controlling the size and morphologies of these magnetic CoNi hierarchical structures.

Figure 9a–c shows the frequency dependence of the complex permittivity real part ε', permittivity imaginary part ε'',

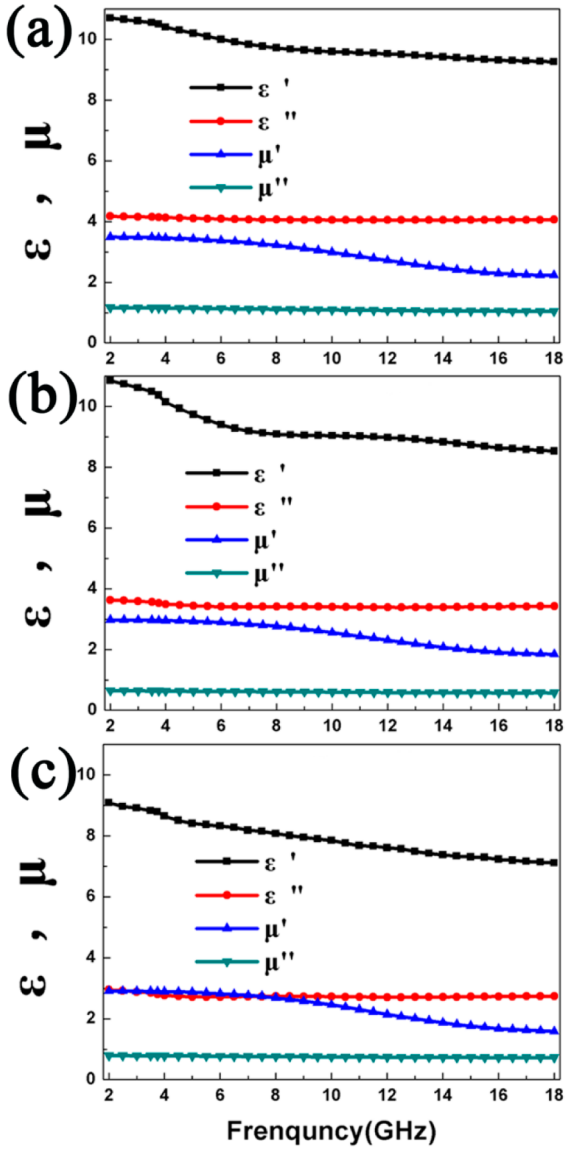

Figure 9. Frequency dependency of real and imaginary parts of complex permittivity (ε) and permeability (μ) of CoNi microflowers with different sizes: (a) 0.6 μm, (b) 1.3 μm, (c) 2.5 μm.

permeability real part μ', and permeability imaginary part μ'' of the CoNi microflowers of different sizes. Considering that CoNi alloys are typical magnetic materials, the permeability real part μ' and imaginary part μ'' of samples have been investigated to understand mechanisms for microwave absorption. The μ'' values of all samples maintain constant, indicating that the energy storage density of these CoNi microflowers is stable in the frequency region between 2 and 18 GHz. On the other hand, the values of μ' obviously reduced as frequency increased from 8 to 18 GHz, which may be caused by the hysteresis effect of the ferromagnetic domain walls and magnetic induction intensity, and consequently demonstrate the magnetic hysteresis loss has actually played a dominant role in microwave absorption behaviors of these CoNi microflowers of different sizes.

The magnetic tangent loss ($\tan \delta\mu = \mu''/\mu'$) represents the capability of magnetic materials to dissipate microwave energy. Figure 10a shows the frequency dependent magnetic tangent

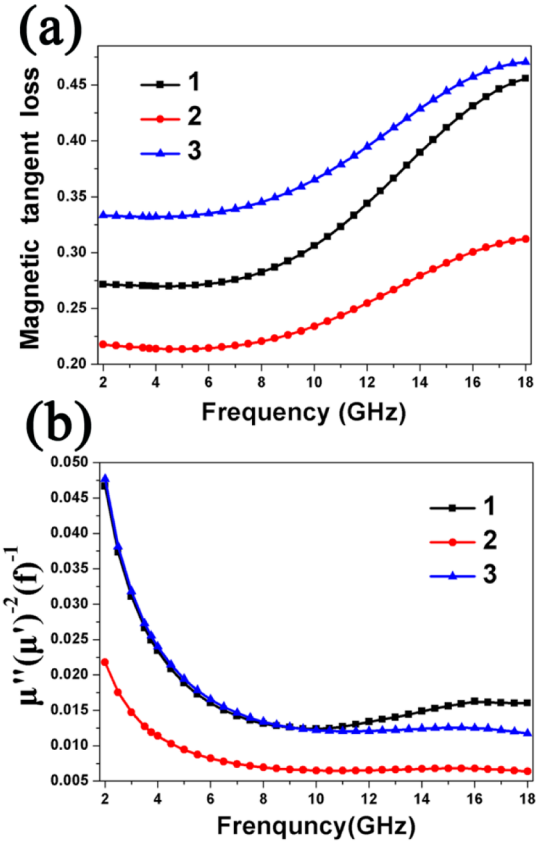

Figure 10. Frequency dependency of the (a) magnetic tangent loss curves and (b) eddy-current loss curves of CoNi microflowers with different sizes. (1:0.6, 2:1.3, and 3:2.5 μm)

loss of as-obtained CoNi microflowers. All samples demonstrate similar elevating trend in the frequency region of 2–18 GHz, implying that they have strong capability to dissipate energy of microwaves. Additionally, the eddy-current loss is dominant for understanding microwave absorption properties. If the magnetic loss is resulted from eddy-current effect, the value of $\mu''(\mu')^{-2}(f)^{-1}$ would be constant and independent of the frequency.[22] Generally, the eddy-current loss is mainly located in high frequency region over 10 GHz for most samples. However, Figure 10b implies that the 0.6 and 2.5 μm CoNi microflower samples have constant $\mu''(\mu')^{-2}(f)^{-1}$ values from 8 to 18 GHz, indicating that the eddy-current loss range of our samples is wider in relatively high frequency region. Therefore, it is obvious that the hierarchical surface structures of CoNi microflowers have a substantial and important effect on their microwave absorption properties.

4. CONCLUSIONS

In conclusion, we have successfully synthesized a series of CoNi microflowers with uniform while different sizes via a facile one-step process. The morphology and size can be controlled by adjusting the concentration of precursors and surfactant. XRD

DOI: 10.1021/am508527s
ACS Appl. Mater. Interfaces 2015, 7, 4233–4240

pattern shows that the prepared CoNi microflowers have a fcc crystal structure and the SEM and TEM images have together revealed their size and uniformity, as well as surface architectures of pristine nanoflakes. Electron holography analysis reveals that the strong stray magnetic fields of CoNi microflowers were actually resulted from their surface nanoflakes. Besides, the 2.5 μm flowers show the highest Ms value of 89.45 emu/g at 300 K, while the largest Hc value of 221.85 Oe is recorded form 0.6 μm flowers at 5 K, and with the size of CoNi flowers increased, Hc decreased but Ms increased. Also, Ms and Hc values at 5 K are higher than those at 300 K. FC/ZFC curves indicate that T_B decreased as size increased, suggesting that the larger flowers need less thermal energy to overcome intrinsic energy barrier. At last, 2.5 μm CoNi microflowers exhibit the strongest microwave absorption ability (−28.5 dB), while 0.6 μm flowers possess the largest absorption bandwidth (6.5 GHz), and as the size of CoNi flowers increased, the RL_{max} was enhanced and corresponding frequency band shifted to lower frequency region. Hence, overall, it is quite possible that these CoNi microflowers with tunable size and surface architectures presented in this work can be tailored for novel high-performance microwave absorption materials in the future.

■ ASSOCIATED CONTENT

Supporting Information

XRD patterns; STEM elemental mapping profiles; SEM/EDS elemental mapping profiles and EDS spectra of a single particle of CoNi microflowers; SEM and TEM images of CoNi microflowers; the magnetic field originating from the nanoflake. This material is available free of charge via the Internet at http://pubs.acs.org.

■ AUTHOR INFORMATION

Corresponding Author

*E-mail: rcche@fudan.edu.cn.

Author Contributions

§Q. Liu and Q. Cao contributed equally to this work.

Notes

The authors declare no competing financial interest.

■ ACKNOWLEDGMENTS

This work was supported by the Ministry of Science and Technology of China (973 Project No. 2013CB932901), and the National Natural Foundation of China (Nos. 11274066, 51172047, 51102050, U1330118). This project was sponsored by Shanghai Pujiang Program and "Shu Guang" project of Shanghai Municipal Education Commission and Shanghai Education Development Foundation (09SG01).

■ REFERENCES

(1) Yang, J.; Zhang, J.; Liang, C. Y.; Wang, M.; Zhao, P. F.; Liu, M. M.; Liu, J. W.; Che, R. C. Ultrathin $BaTiO_3$ Nanowires with High Aspect Ratio: A Simple One-Step Hydrothermal Synthesis and Their Strong Microwave Absorption. *ACS Appl. Mater. Interfaces* **2013**, *5*, 7146−7151.

(2) Zhao, P. F.; Liang, C. Y.; Gong, X. W.; Gao, R.; Liu, J. W.; Wang, M.; Che, R. C. Microwave Absorption Enhancement, Magnetic Coupling and *ab Initio* Electronic Structure of Monodispersed $(Mn_{1-x}Co_x)_3O_4$ Nanoparticles. *Nanoscale* **2013**, *5*, 8022−8028.

(3) Cao, Q.; Liu, Z. W.; Che, R. C. Ordered Mesoporous $CoFe_2O_4$ Nanoparticles: Molten-Salt-Assisted Rapid Nanocasting Synthesis and the Effects of Calcining Heating Rate. *New J. Chem.* **2014**, *38*, 3193−3198.

(4) Yang, X. C.; Wang, Z.; Jing, M. X.; Liu, R. J.; Song, F. Z.; Shen, X. Q. Magnetic Nanocomposite Ba-Ferrite/alpha-Iron Hollow Microfiber: A Multifunctional 1D Space Platform for Dyes Removal and Microwave Absorption. *Ceram. Int.* **2014**, *40*, 15585−15594.

(5) Zhao, B.; Shao, G.; Fan, B. B.; Chen, Y. Q.; Zhang, R. Effect of the TiO_2 Amounts on Microwave Absorption Properties of Ni/TiO_2 Heterostructure Composites. *Physica B* **2014**, *454*, 120−125.

(6) Kurlyandskaya, G. V.; Bhagat, S. M.; Luna, C.; Vazquez, M. Microwave Absorption of Nanoscale CoNi Powders. *J. Appl. Phys.* **2006**, *99*, 104308.

(7) Toneguzzo, P.; Viau, G.; Acher, O.; Fievet-Vincent, F.; Fievet, F. Monodisperse Ferromagnetic Particles for Microwave Applications. *Adv. Mater.* **1998**, *10*, 1032.

(8) Feng, W. Q.; Yang, L.; Cao, N.; Du, C.; Dai, H. M.; Luo, W.; Cheng, G. Z. *In Situ* Facile Synthesis of Bimetallic CoNi Catalyst Supported on Graphene for Hydrolytic Dehydrogenation of Amine Borane. *Int. J. Hydrogen Energy* **2014**, *39*, 3371−3380.

(9) Liu, Q.; Guo, X.; Wang, T.; Li, Y.; Shen, W. Synthesis of CoNi Nanowires by Heterogeneous Nucleation in Polyol. *Mater. Lett.* **2010**, *64*, 1271−1274.

(10) Ahmed, J.; Sharma, S.; Ramanujachary, K. V.; Lofland, S. E.; Ganguli, A. K. Microemulsion-Mediated Synthesis of Cobalt (Pure FCC and Hexagonal Phases) and Cobalt-Nickel Alloy Nanoparticles. *J. Colloid Interface Sci.* **2009**, *336*, 814−819.

(11) Ergeneman, O.; Sivaraman, K. M.; Pané, S.; Pellicer, E.; Teleki, A.; Hirt, A. M.; Baró, M. D.; Nelson, B. J. Morphology, Structure and Magnetic Properties of Cobalt−Nickel Films Obtained from Acidic Electrolytes Containing Glycine. *Electrochim. Acta* **2011**, *56*, 1399−1408.

(12) Hu, M. J.; Lu, Y.; Zhang, S.; Guo, S. R.; Lin, B.; Zhang, M.; Yu, S. H. High Yield Synthesis of Bracelet-Like Hydrophilic Ni-Co Magnetic Alloy Flux-Closure Nanorings. *J. Am. Chem. Soc.* **2008**, *130*, 11606−11607.

(13) Wu, H. Q.; Cao, P. P.; Li, W. T.; Ni, N.; Zhu, L. L.; Zhang, X. J. Microwave-Assisted Synthesis and Magnetic Properties of Size-Controlled CoNi/MWCNT Nanocomposites. *J. Alloys Compd.* **2011**, *509*, 1261−1265.

(14) Cao, Q.; Che, R. C. Tailoring Au−Ag−S Composite Microstructures in One-Pot for Both SERS Detection and Photocatalytic Degradation of Plasticizers DEHA and DEHP. *ACS Appl. Mater. Interfaces* **2014**, *6*, 7020−7027.

(15) Zhang, L.; Bain, J. A.; Zhu, J. G.; Abelmann, L.; Onoue, T. The Role of MFM Signal in Mark Size Measurement in Probe-Based Magnetic Recording on CoNi/Pt Multilayers. *Physica B* **2007**, *387*, 328−332.

(16) Elumalai, P.; Vasan, H. N.; Munichandraiah, N.; Shivashankar, S. A. Kinetics of Hydrogen Evolution on Submicron Size Co, Ni, Pd and CoNi alloy Powder Electrodes by D.C. Polarization and A.C. Impedance Studies. *J. Appl. Electrochem.* **2002**, *32*, 1005−1010.

(17) Liu, Q. H.; Xu, X. H.; Xia, W. X.; Che, R. C.; Chen, C.; Cao, Q.; He, J. G. Dependency of Magnetic Microwave Absorption on Surface Architecture of $Co_{20}Ni_{80}$ Hierarchical Structures Studied by Electron Holography. *Nanoscale* **2015**, *7*, 1736−1743.

(18) Lu, W. H.; Sun, D. B.; Yu, H. Y. Synthesis and Magnetic Properties of Size-Controlled CoNi Alloy Nanoparticles. *J. Alloys Compd.* **2013**, *546*, 229−233.

(19) Zhou, W.; Zheng, K.; He, L.; Wang, R. M.; Guo, L.; Chen, C. P.; Han, X.; Zhang, Z. Ni/Ni_3C Core-Shell Nanochains and Its Magnetic Properties: One-Step Synthesis at Low Temperature. *Nano Lett.* **2008**, *8*, 1147−1152.

(20) Castrillon, M.; Mayoral, A.; Magen, C.; Meier, J. G.; Marquina, C.; Irusta, S.; Santamaria, J. Synthesis and Characterization of Ultra-Small Magnetic FeNi/G and NiCo/G Nanoparticles. *Nanotechnology* **2012**, *23*, 085601.

(21) Liu, J. W.; Xu, J. J.; Che, R. C.; Chen, H. J.; Liu, Z. W.; Xia, F. Hierarchical Magnetic Yolk-Shell Microspheres with Mixed Barium

DOI: 10.1021/am508527s
ACS Appl. Mater. Interfaces 2015, 7, 4233−4240

Silicate and Barium Titanium Oxide Shells for Microwave Absorption Enhancement. *J. Mater. Chem.* **2012**, *22*, 9277−9284.
(22) Wang, H.; Dai, Y. Y.; Gong, W. J.; Geng, D. Y.; Ma, S.; Li, D.; Liu, W.; Zhang, Z. D. Broadband Microwave Absorption of CoNi@C Nanocapsules Enhanced by Dual Dielectric Relaxation and Multiple Magnetic Resonances. *Appl. Phys. Lett.* **2013**, *102*, 223113.

DOI: 10.1021/am508527s
ACS Appl. Mater. Interfaces 2015, 7, 4233−4240